

Shock heating in the group atmosphere of the radio galaxy B2 0838+32A

Nazirah N. Jetha^{1*}, Martin J. Hardcastle², Trevor J. Ponman³ and Iринi Sakelliou⁴

¹Laboratoire AIM, CEA/DSM - CNRS - Université Paris Diderot, DAPNIA/Service d'Astrophysique, Bât. 709, CEA-Saclay, F-91191 Gif-sur-Yvette Cédex, France

²School of Physics, Astronomy and Mathematics, University of Hertfordshire, College Lane, Hatfield, Hertfordshire AL10 9AB

³School of Physics and Astronomy, University of Birmingham, Edgbaston, Birmingham B15 2TT

⁴Max-Planck-Institute für Astronomie, Königstuhl 17, D-69117 Heidelberg, Germany

ABSTRACT

We present *Chandra* and radio observations, and analysis of Sloan Digital Sky Survey data, of the radio galaxy B2 0838+32A (4C 32.26) and its environment. The radio galaxy is at the centre of a nearby group that has often been identified with the cluster Abell 695, but we argue that the original Abell cluster is likely to be an unrelated and considerably more distant system. The radio source is a restarting radio galaxy and, using our *Chandra* data, we argue that the currently active lobes are expanding supersonically, driving a shock with Mach number $2.4^{+1.0}_{-0.5}$ into the inter-stellar medium. This would be only the third strong shock round a young radio source to be discovered, after Centaurus A and NGC 3801. However, in contrast to both these systems, the host galaxy of B2 0838+32A shows no evidence for a recent merger, while the AGN spectrum shows no evidence for the dusty torus that would imply a large reservoir of cold gas close to the central black hole. On the contrary, the AGN spectrum is of a type that has been associated with the presence of a radiatively inefficient accretion flow that could be controlled by AGN heating and subsequent cooling of the hot, X-ray emitting gas. If correct, this means that B2 0838+32A is the first source in which we can directly see entropy-increasing processes (shocks) driven by accretion from the hot phase of the interstellar medium.

Key words:

1 INTRODUCTION

Recent observations of galaxy groups and clusters have highlighted two major, and as yet unresolved, problems in our understanding of the formation and evolution of these objects. The first is that of similarity breaking; whilst groups and clusters do follow well studied scaling relations, they differ significantly from those derived from models of self-similar gravitational collapse (e.g. Sanderson et al. 2003, Popesso et al. 2005). The second problem is that many of these systems exhibit cores of cool gas with cooling times well below the Hubble time. In theory, these cool cores should have cooled to such temperatures that they are no longer visible in the X-ray; however, no evidence of such cool gas is found (e.g. Peterson et al. 2001, Sakelliou et al. 2002). The heating mechanism is still the subject of vigorous debate, but there is increasing evidence that active galactic nucleus (AGN) outbursts could heat the intergalactic medium (IGM). Depending on the scale of the outburst, not only could they prevent catastrophic cooling in the core, but over repeated cycles of activity outbursts may also inject sufficient extra energy at larger radii to drive groups and clusters away from the predicted self-similar scaling relations.

The heating on small scales can be achieved by shock heating of the IGM by the rapidly expanding small-scale lobes of a radio-loud AGN (Kraft et al. 2003), whilst the larger scale heating may be the result of the evolution of buoyant bubbles (Reynolds et al. 2002, Nusser et al. 2006, for simulations; Bîrzan et al. 2004, Clarke et al. 2005, for observations). In the simulations, overpressured bubbles of radio plasma that have evolved from old, dead radio galaxies and which are light compared to the IGM, rise due to buoyancy. As they rise, they expand and heat the IGM as the bubbles come into pressure equilibrium (e.g. Begelman 2001). Alternatively, large scale heating may also arise from the interactions between the radio jets and the IGM (Heinz et al. 2006), or from the dissipation of large-scale shocks such as those seen in Perseus A (Fabian et al. 2006) and Hydra A (Nulsen et al. 2005). The models therefore predict that we should expect to see several different phases of AGN heating, and, in the rare sources in which there is clear evidence for multiple AGN outbursts, we might expect to see more than one such process operating at once.

However, the cumulative effect of AGN heating is not well understood observationally, since there are very few systems that show evidence of multiple AGN outbursts. This makes examining the energy output of a radio source at different stages of its evolution, whilst keeping the external environment more or less consis-

* E-mail: nazirah.jetha@cea.fr

tent, rather difficult. Finding evidence of multiple outbursts in the same system, from the same host galaxy, allows us firstly to investigate the energy output of the radio source at different stages of its lifetime and secondly to determine how this energy can be coupled to the IGM at different points in the radio galaxy’s evolution. Furthermore, observing systems with multiple visible outbursts may provide information as to how successive outbursts affect the IGM and how a radio galaxy may, at different points in its evolution, perform different functions; i.e. in the early, overpressured stages of evolution, the source may have sufficient energy to increase the central entropy of the system, whilst at later stages, the source may only have sufficient energy to control cooling, and no more. There are, observationally, some indications that repeated AGN outbursts may have an effect on the IGM (e.g. Croston et al. 2005, Jetha et al. 2007); however, in order to investigate fully the questions outlined above, systems showing multiple outbursts are required. Such systems are relatively rare. Firstly to detect such systems, it must be possible to image low surface brightness features in the X-ray or radio; secondly, and more importantly, it must be possible to study the gaseous environments of the sources in detail. Relatively few even of the known multiple-outburst sources meet these criteria.

The few well-studied systems that show evidence for multiple AGN outbursts include Centaurus A (Kraft et al. 2003), M87 (Owen et al. 2000) Perseus A (Fabian et al. 2003) and Hydra A (Wise et al. 2007). Cen A does show a strong shock around the inner radio lobes; however, it is an extremely poor, very close system ($kT \simeq 0.3$ keV; $D = 3.7$ Mpc), which, whilst providing an ideal laboratory to study the shock surrounding the new, young radio source, does not provide a suitable environment for studying the long term effects of the older outbursts, due to the paucity of gas in the outer regions and the large angular scale of the oldest radio structures. M87, Perseus A and Hydra A, on the other hand, are highly complex systems, showing signs of multiple generations of outbursts, which makes it difficult to disentangle the effects of successive outbursts. Further, in all these cases, the youngest components of the radio sources are relatively mature, and past the shock-heating stage. The only other published example of a strong shock around a young radio source is NGC 3801 (Croston et al. 2007), which, like Cen A, is a low-temperature ($kT = 0.23$ keV) system in an elliptical galaxy that has recently undergone a major merger. However, there is little evidence in this system of multiple AGN outbursts, which are required in order to investigate the issues raised above.

In this paper we present *Chandra* observations of the radio source B2 0838+32A, otherwise known as 4C 32.26. This object first came to our attention as a potential wide-angle tailed radio source (WAT) during preliminary study of Abell clusters for the work of Jetha et al. (2006). Upon closer investigation of the radio data we found that the source was not a WAT, but rather a restarting radio source, showing evidence for two distinct epochs of radio activity, which prompted our *Chandra* observations. We begin the present paper by resolving a long-standing confusion about the association of this object with an Abell cluster. In the literature, the host galaxy of the radio source has been presented as the brightest cluster galaxy (BCG) of Abell 695 (e.g. Fanti et al. 1978), but there is an 8-arcmin separation between the position of the radio galaxy and the catalogued position of the Abell cluster (Abell et al. 1989). In Section 2 of the present paper we discuss the true environment of the radio source. We then discuss the details of the radio observations used in the paper in Section 3. In Section 4 we present our new *Chandra* observation and in Section 5 we discuss the details of the IGM. Our analysis of the structures seen in the *Chandra* data

Table 1. Positions and velocities of the galaxies used to determine the redshift and velocity dispersion of the Abell 695 group. All positions and redshifts are taken from the SDSS Data Release 6. The final column indicates whether the galaxy is a group member as classified by ROSTAT.

Galaxy co-ordinates		z	Group Membership
α_{2000}	δ_{2000}		
08 41 12.79	32 24 55.20	0.0696	
08 41 6.22	32 25 6.79	0.0657	
08 41 21.06	32 24 42.74	0.0696	
08 40 53.81	32 23 46.17	0.0670	Y
08 41 8.89	32 20 38.34	0.0683	Y
08 41 27.35	32 28 33.01	0.0646	
08 41 22.95	32 28 34.81	0.0665	
08 41 29.33	32 24 54.10	0.0656	
08 40 49.25	32 25 1.01	0.0677	Y
08 41 27.72	32 19 41.17	0.0656	
08 41 5.64	32 31 22.76	0.0677	
08 40 40.16	32 22 54.08	0.0684	Y
08 40 12.54	32 14 22.61	0.0683	Y
08 40 37.84	32 12 56.59	0.0672	Y
08 41 50.17	32 26 23.48	0.0542	
08 42 1.38	32 30 28.25	0.0528	
08 41 52.92	32 36 5.98	0.0660	
08 42 13.92	32 33 49.72	0.0532	
08 41 53.93	32 17 57.45	0.0695	Y
08 41 53.57	32 19 59.88	0.0671	Y
08 40 13.80	32 27 52.94	0.0682	Y
08 40 38.97	32 30 27.34	0.0517	
08 40 59.09	32 38 12.39	0.0682	Y
08 40 54.81	32 44 28.21	0.0684	Y
08 42 13.24	32 17 11.07	0.0677	Y
08 40 29.24	32 38 34.96	0.0686	Y

is presented in Section 6, the interpretation of our results in terms of feedback models is given in Section 7 and our conclusions are presented in Section 8.

2 IDENTITY AND REDSHIFT OF THE GROUP HOSTING B2 0838+32A

The radio source B2 0838+32A has traditionally been assumed to reside at the centre of the galaxy cluster Abell 695 (e.g. Fanti et al. 1978), despite the 8 arcmin discrepancy between the co-ordinates of the radio source (08h41m13.1s, +32d25m00s) and the galaxy cluster known as Abell 695 (08h41m24.2s, +32d17m16s), which exceeds the notional 2.5 arcmin uncertainty on the cluster position (Abell et al. 1989). Additionally, the redshift of the radio galaxy has almost always been assumed to be the same as that of the cluster Abell 695, and is cited in the literature as such (e.g. Sandage 1978, Noonan 1981, Feitsova 1981, Sarazin et al. 1982, Struble & Rood 1987, Struble & Rood 1999). This has been further reinforced by the presence of a group of galaxies clustered around B2 0838+32A both spatially and in redshift space (see Table 1).

To determine whether the group associated with the radio galaxy B2 0838+32A and the galaxy cluster Abell 695 are the same entity, we obtained the SDSS DR 6¹ positions and redshifts for all galaxies in a 20 arcmin radius of the catalogued central position of Abell 695, to ensure that galaxies from both Abell 695 and those

¹ <http://cas.sdss.org/astro/en/>

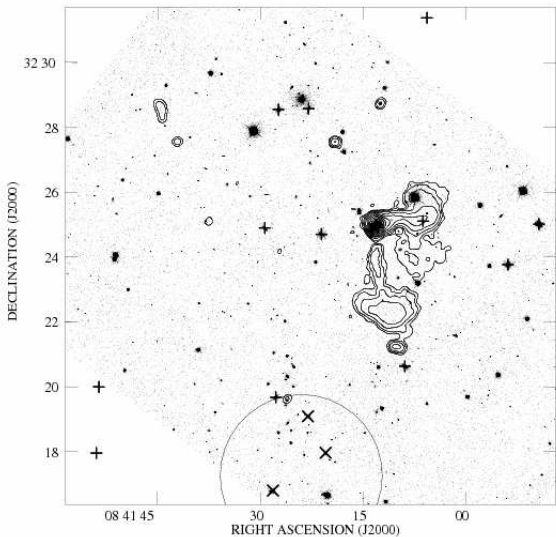


Figure 1. Optical SDSS image of the region overlaid with radio contours of the radio source B2 0838+32A, together with galaxies at the group redshift marked with crosses, galaxies in the range $z = 0.15 - 0.18$ in the cluster region marked with 'x', and the nominal Abell cluster position marked with a large circle. It can be seen that there are two distinct groupings of objects – a nearby group centred around the radio galaxy and a more distant group/cluster at higher redshift.

surrounding the radio galaxy were included. However, examining the SDSS data, whilst it is clear that there is a group of galaxies around B2 0838+32A, this group does not fit with the documented Abell richness classification, in that the documented Abell richness class is 1, indicating that the cluster should contain between 50-79 galaxies in the magnitude range m_3 to $m_3 + 2.0$, where m_3 is the magnitude of the third brightest galaxy, within 1.7 arcmin of the cluster centre (Abell 1958). As we have only 26 galaxies in total within 10 arcminutes of the radio source, and the radio source is offset by 8 arcmin from the central position of the Abell cluster, we propose instead that the group of galaxies centred around B2 0838+32A is a real foreground group, whilst the original system identified by Abell is a cluster of galaxies centred approximately 8 arcmin south of B2 0838+32A at a much higher redshift. This has been suggested in the past by Sarazin et al. (1982), who calculated a photometric redshift of 0.152 for the cluster of galaxies at the catalogued position of Abell 695.

In Figure 1, we show the optical image together with positions (with the redshift range indicated by the different symbols) for all galaxies within a 20 arcmin radius of the nominal centre of Abell 695. It is immediately clear that there are in fact two overdensities of galaxies, which whilst appearing to be adjacent/overlapping in projection, are greatly separated in redshift space. Using ROSTAT (Beers et al. 1990), a $3 - \sigma$ clipping algorithm, we were able to determine average redshifts and velocity dispersions for the closer system, but there were insufficient redshift measurements to allow us to do the same for the more distant system, which we estimate, using the available SDSS redshifts for this system, to be in the redshift range 0.15-0.18, consistent with the estimate of Sarazin et al. (1982).

For the closer system, we used SDSS redshifts of objects within a radius of 10 arcmin of the radio galaxy in the redshift range $0.06 \leq z \leq 0.078$ (the redshift of the radio galaxy is 0.068), a total of 26 objects in all (all of which fall within the 20 arcmin radius ini-

tially investigated), as detailed in Table 1. We then applied the ROSTAT algorithm to this list of redshifts in order to determine a mean redshift and velocity dispersion. The algorithm rejected 14 of the objects on the basis of $3 - \sigma$ clipping, leaving us with the 12 objects marked. We obtained $z_{ave} = 0.0682$ and $\sigma_{grp} = 300_{-50}^{+100}$ km s⁻¹ for this foreground system², which henceforth, for simplicity, we will call ‘the 0838+32A group’, in contrast to the more distant Abell 695 cluster. For the remainder of this paper, we take the redshift of the 0838+32A group, and the radio galaxy it hosts, to be 0.068, which corresponds to a luminosity distance of 300 Mpc in standard Λ CDM cosmology, $H_0 = 71$ km s⁻¹ Mpc⁻¹; in this cosmology 1 arcsec corresponds to 1.29 kpc.

3 RADIO OBSERVATIONS AND SPECTRA

We reduced archival 1.4 and 4.8 GHz VLA observations (details given in Table 2) of the object B2 0838+32A in AIPS in the usual way. The low resolution 1.4 GHz map shows a compact central source embedded in large-scale diffuse emission. The 4.9-GHz images show the large-scale structure seen in the 1.4-GHz map and also resolve the compact inner source as shown in Fig 2 (inset). The bright, compact double lobes of the inner source, with a total physical scale of 16 kpc, are characteristic of a young radio galaxy, but the outer lobes, which are a factor ~ 3 times fainter at 1.4 GHz and each extend ~ 250 kpc from the nucleus, are unusual; they both appear to show a jet leading into a broad, faint lobe, but the ‘jets’ are at 90° to each other in projection, and show no apparent connection to the inner lobes, a situation reminiscent of the large-scale ‘jet’ between the inner lobes and north middle lobe in Cen A (Morganti et al. 1999). As the 4.7-GHz D-configuration data have similar uv plane coverage to the 1.4-GHz C-configuration, we were able to measure spectral indices for various components of the source (for this comparison we discarded the short baselines that are present in the 1.4-GHz but not the 4.7-GHz dataset to reduce bias). We found that the inner lobes have $\alpha_{1.4}^{4.7} = 0.65$ while the outer lobes both have $\alpha_{1.4}^{4.7} = 1.0$: qualitatively this is consistent with the idea that the outer lobes are relics of an earlier outburst. The faint low-surface-brightness southern region of the W lobe is not detected in the 4.7-GHz data and may be presumed to be steeper-spectrum still. The large-scale ‘jets’ have intermediate spectral indices.

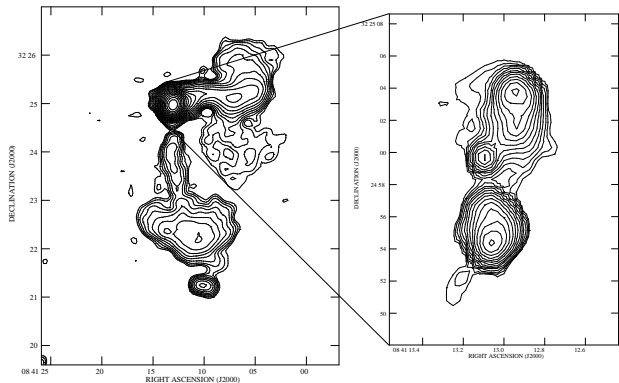
Fitting Jaffe & Perola (1973) spectral aging models to the lobes assuming an original spectral index of $\alpha = 0.55$ (from comparison with measurements from currently active FRI lobes), we found that the maximum spectral age of the lobes (Leahy 1991) is around 5×10^7 years. Losses to inverse-Compton scattering dominate for plausible (equipartition or sub-equipartition) magnetic field strengths. As usual, spectral aging timescales of this kind assume passive evolution of the electron population after the original population has been set up; thus it is probably best to interpret this age as a lower limit on the age of the lobe, assuming that since the lobes are likely to be in approximate pressure balance with the IGM, there has been little expansion since the energy supply was discontinued.

The minimum pressure (assuming a fully tangled magnetic

² Our value of σ is consistent within the joint errors with the somewhat higher value, also determined from SDSS data, that is tabulated by Aguerri et al. (2007). The data they present are insufficient to show which galaxies were used in their analysis and so a more detailed comparison of their results with ours is not possible.

Table 2. Details of the VLA radio datasets used in this work.

Obs. ID	Array Configuration	Frequency (GHz)	Observation date	Observation duration (mins)
AM364	B	4.9	1993-03-28	56
AV265	D	4.7	2003-04-11	250
AV265	C	1.4	2004-04-10	180

**Figure 2.** 1.4-GHz VLA image of the radio source (main image) of resolution 14.25×13.02 arcsec, showing the large-scale radio lobes; the inner lobes appear unresolved in this image. The inset image is a 1.09×0.98 arcsec, 4.9-GHz image that shows the inner core and lobes. Contours are in $\sqrt{2}$ steps with the lowest contour at $0.31 \text{ mJy beam}^{-1}$ for both images.

field so that $P = (U_e + U_B)/3$ in the large-scale lobes is of the order of $1.2 \times 10^{-14} \text{ Pa}$, while in the inner lobes it is $6 \times 10^{-12} \text{ Pa}$.

4 X-RAY OBSERVATIONS

The galaxy group was observed with *Chandra* in two separate observations (see Table. 3 for details) and processed following the *CIAO* online threads, applying the latest calibration products, removing bad pixels and excluding periods of high background. After data cleaning, we were left with good time intervals of 59.7 and 21.6 ks giving a total clean exposure time of 81.3 ks. A merged data file was created for spatial analysis, but following *CIAO* recommendations, the spectral analysis was carried out by extracting spectra separately from each events file and fitting models to them jointly. We use XSPEC 12 for spectral fitting.

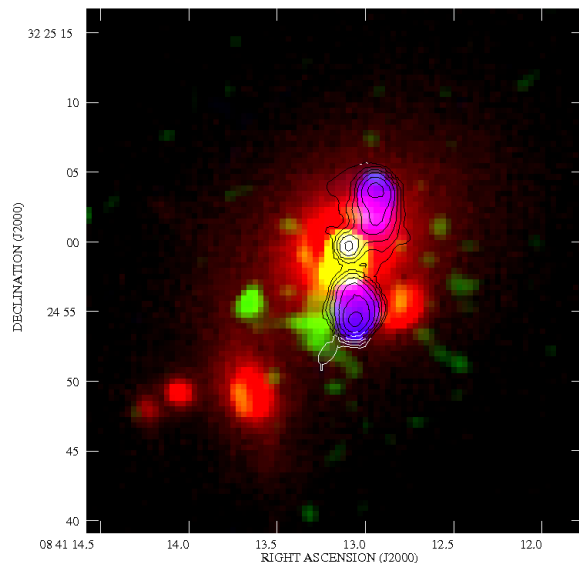
5 X-RAY ANALYSIS

5.1 Spatial Analysis

At first glance, the 0.5-5.0 keV X-ray image shows the AGN and some small-scale diffuse emission, with structure surrounding the

Table 3. Details of the *Chandra* X-ray observations used in this work.

Observation ID	Observation date	Unfiltered exposure time (ks)	Filtered exposure time (ks)
7917	2006-12-27	61	59.7
8500	2006-12-30	21.8	21.6

**Figure 3.** 3 colour image incorporating the SDSS R-band data (red channel), *Chandra* X-ray data (green channel), and VLA 4.8 GHz radio data (blue channel), overlaid with the VLA A-Array 4.8 GHz radio contours to highlight the radio lobes. It can be seen that the radio lobe is contained entirely within the BGG of the group and that the X-ray emission is enhanced in the SE edge of the lobe, but from the SDSS image, it is clear that the X-rays are being emitted from the region in between the main galaxy and its smaller companion to the SE. The X-ray data are binned in standard *Chandra* pixels (0.492 arcsec) and smoothed with a Gaussian of FWHM of 0.5 arcsec. The radio contours are at $0.25 \times (\sqrt{2}, 2\sqrt{2}, \dots) \text{ mJy beam}^{-1}$

south-eastern edge of the southern radio lobe (see Fig. 3), but very little large-scale emission can be detected by eye. To test for the presence of any large scale emission, we created the surface brightness profile shown in Fig. 4. This profile seems to show structure on several scales: the large-scale emission is not well fitted with a single β model. We therefore fitted it with a projected double β -model as described by Croston et al. (2008), using the Markov-Chain Monte Carlo parameter space searching algorithm described in that paper with uniform priors on β values and Jefferys priors on scale parameters. The best-fitting (maximum-likelihood) model is plotted with the data in Fig. 4. The parameters of the larger-scale component of the double β model are not well constrained (unsurprisingly, as it is represented by only the few outer bins of our surface brightness profile) but the data do allow us to constrain the density and thus the pressure (assuming a temperature, see Section 5.2) of thermal material on the scales covered by the radial profile (Fig. 5).

In order to ascertain how typical the IGM is (e.g. to be able to make statements about any heating of the IGM by the radio source), we scaled the surface brightness profile radially and vertically by R_{500} and compared the profile of the Abell 695 group with that of other similarly scaled nearby groups taken from Jetha et al. (2007). To determine R_{500} for the Abell 695 group, we used a temperature of 0.7 keV (see Section 5.2) and the scaling relation $R_{500} = 391 \times T^{0.63}$ from Willis et al. (2005), which we determine to be 310 kpc. We find that the Abell 695 group is not significantly different to other local groups, and that the lack of easily detectable emission is due to the ACIS-S background.

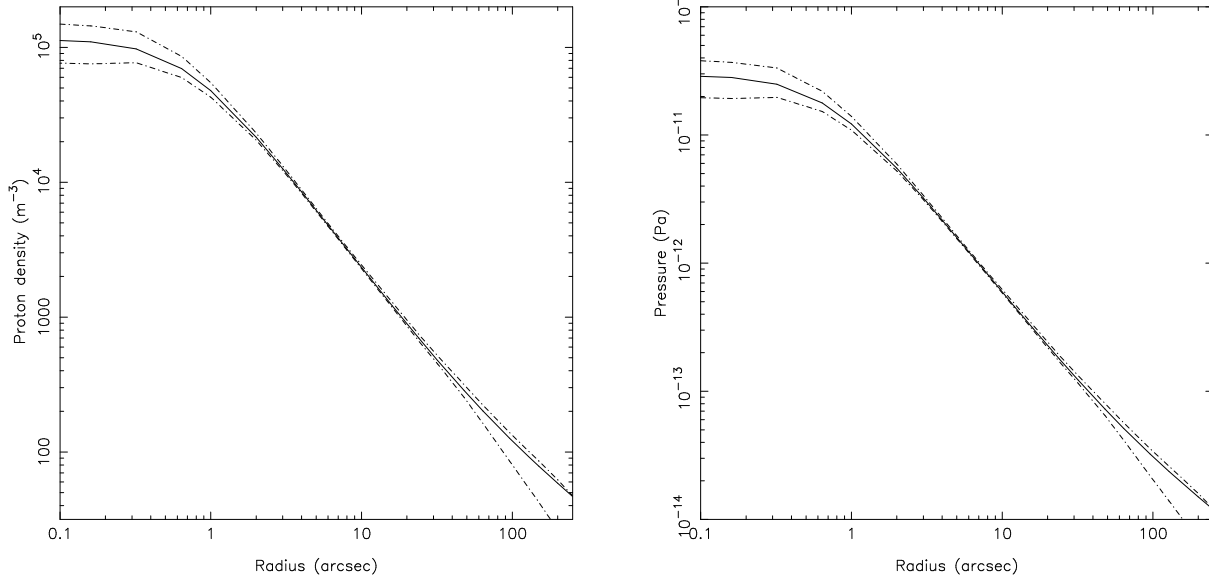


Figure 5. The inferred density and pressure profiles for the group derived from fitting of the double β model described in the text. The solid line shows the Bayesian estimate of each quantity, and the dashed-dotted lines show the 68% confidence intervals (formally credible intervals) around the estimate. A temperature of 0.7 keV is assumed for the gas and the errors on the pressure profile do not take into account the uncertainty on this value of temperature.

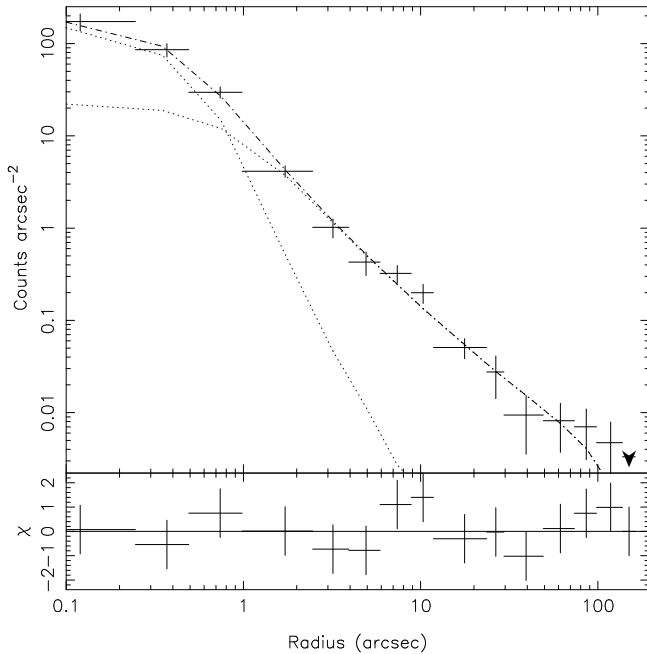


Figure 4. The surface brightness profile of the A695 group and central galaxy. The dotted lines show the two components of the fitted model, consisting of a point source and the double β model described in the text, both convolved with the *Chandra* PSF, and the dashed line shows their sum. The residuals (data minus model) in terms of the contribution to χ^2 are also plotted.

5.2 Temperature of the group

We extracted spectra from both events files in the same region as used for the surface brightness analysis in Section 5.1, with a local background (for each file) for background subtraction, and excluded a region 7 arcsec (9 kpc) in radius to mask out the con-

tribution from the brightest group galaxy (BGG) and extended small-scale structure. Each spectrum was binned such that each bin contained 200 counts after background subtraction. Examining the spectra from each observation in turn, and considering the faintness of the source, we found that the emission above 2.5 keV in observation 7919 was dominated by background, whilst the emission at all energies in observation 8500 was dominated by the background. Thus, for the spectral fitting of the group, we use only observation 7919 in the energy range 0.5–2.5 keV. We fitted the spectrum with an absorbed APEC model with abundance fixed to $0.3Z_{\odot}$. This fit gave a global group temperature of 0.7 ± 0.1 keV with reduced chi-squared, $\chi^2_{\nu} = 0.9$ for 21 d.o.f. We give details of this fit in Table 4, and show the fitted spectrum in Fig 6.

To check the veracity of this result, since the spectrum is rather noisy, we checked the temperature in two ways. First, we extracted a spectrum from the entire region, including the BGG (but not the central AGN, which we exclude using a region of radius 2.5 arcsec) and surroundings (to provide a better SNR), and a separate spectrum from simply the BGG (but again with the AGN excluded) and surroundings. We fitted the BGG spectrum with two absorbed APEC models (one each for the galaxy and the extended structure), as detailed in Table 5, and then used these fitted parameters as a model for the galaxy and shock in the group spectrum. Modeling the galaxy and shock and fitting a further APEC model to the global spectrum resulted in a temperature of 0.7 ± 0.2 keV with $\chi^2_{\nu} = 0.8$ for 21 d.o.f., in agreement with the temperature found when excluding the galaxy emission.

We further estimate the temperature based on the $\sigma - T_X$ relation of Osmond & Ponman (2004). From the SDSS data in Section 2, we calculated that $\sigma_{grp} = 300^{+100}_{-50}$ km s⁻¹, and using this velocity dispersion, we find that the predicted temperature is $0.5^{+0.5}_{-0.2}$ keV, in agreement with our spectral measurements of the group temperature.

Thus, taking these multiple temperature estimates into account, we adopt a temperature of 0.7 keV for the group. A summary of our temperature estimates are tabulated in Table 6. We also plot

Table 4. Details of the spectral model fitted to the group.

Component	Parameter	Value
wabs	N_{H}	$3.96 \times 10^{20} \text{ cm}^{-2}$
APEC	kT	$0.7 \pm 0.1 \text{ keV}$
	N	$(5.4 \pm 0.9) \times 10^{-5}$
L_X (unabsorbed)		$(3.2 \pm 0.2) \times 10^{42} \text{ erg s}^{-1}$
χ^2 (d.o.f.)		8.3 (9)

Table 5. Details of the spectral model fitted to the galaxy and surrounding structure.

Component	Parameter	Value
wabs	N_{H}	$3.96 \times 10^{20} \text{ cm}^{-2}$
APEC	kT	$0.2^{+0.4}_{-0.1} \text{ keV}$
	N	$(1.5 \pm 0.5) \times 10^{-5}$
APEC (shock)	kT	$1.9^{+0.8}_{-0.3} \text{ keV}$
	N	$(1.1 \pm 0.2) \times 10^{-4}$
χ^2 (d.o.f.)		18.9 (21)

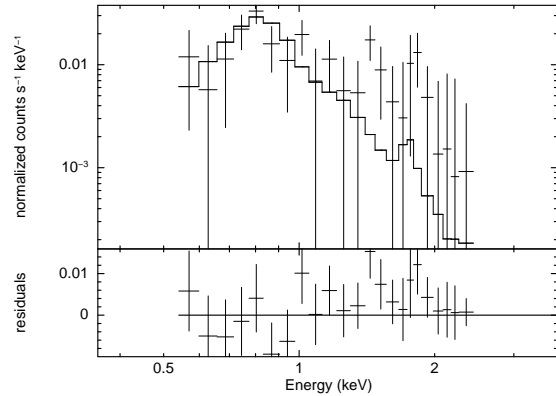
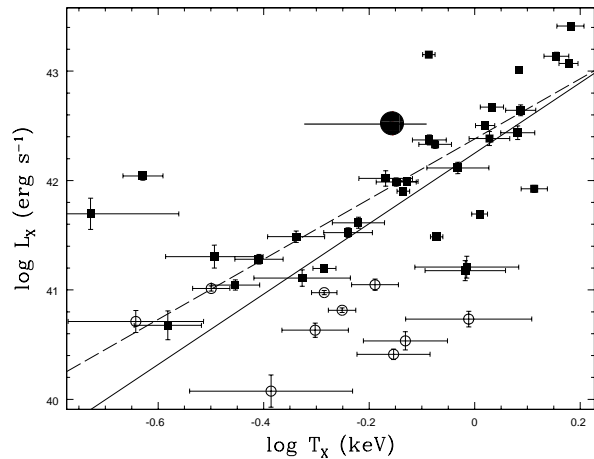
the group on the $L_X : T_X$ relation of Osmond & Ponman (2004), as shown in Fig. 7 using an X-ray temperature of $0.7 \pm 0.1 \text{ keV}$ and the unabsorbed X-ray luminosity given in Table 4, and the group does not show any significant deviation from the $L_X : T_X$ relation.

5.3 Spectrum of the AGN

In order to be able to compare the nuclear properties of the radio galaxy with other sources that are known to drive strong shocks through the IGM, we extracted a spectrum of the AGN, centred on the radio core and extending out to 2.5 arcsec. For the background, a similar sized region was used, positioned so as to avoid the region of hot gas to the SE. We fitted the spectrum in the energy range 0.4–7.0 keV with an absorbed power law model, and initially fixed the absorption to the Galactic value, resulting in a power-law with photon index, $\Gamma = 1.7 \pm 0.2$, with $\chi^2_{\nu} = 1.2$ (for 6 d.o.f.). Fitting a model similar to that used for Cen. A provides a worse fit ($\chi^2_{\nu} = 2.2$ for 3 d.o.f.), indicating that the nuclear spectrum for this source requires a simple power law only. We find that the 1-keV nuclear X-ray flux density from the power law is $2.1 \pm 0.3 \text{ nJy}$. Comparing the X-ray and 5-GHz nuclear fluxes and luminosities (see Section 3) with the analysis of Evans et al. (2006), we find that the core properties of B2 0838+32A are entirely consistent with both the radio and X-ray components being emission from the unresolved bases of jets, and could also indicate the presence of a radiatively inefficient accretion flow (e.g. Donato et al. 2004), and a complete absence of a torus.

Table 6. A summary of our various temperature estimates

Method	Temperature
Direct fitting to group spectrum	$0.7 \pm 0.1 \text{ keV}$
Modeling shock and galaxy component and fitting group spectrum	$0.7 \pm 0.2 \text{ keV}$
Using $\sigma - T_X$ relation of Osmond & Ponman (2004)	$0.5^{+0.5}_{-0.2} \text{ keV}$

**Figure 6.** Spectrum of the group, excluding the shock and BGG extracted from the 7919 observation only and fitted in the energy range 0.5–2.5 keV with an absorbed APEC model. We find a temperature of $0.7 \pm 0.1 \text{ keV}$ for the group from this spectrum**Figure 7.** $L_X : T_X$ relation taken from Osmond & Ponman (2004); the solid line represents the fit to their entire sample and the dashed line the fit to only those systems which show large-scale extended emission. The open points represent those sources without large scale extended emission, whilst the closed points show those systems with extended halos. The X-ray properties of the B2 0838+32A group are indicated by the large black point.

6 THE FEATURE TO THE SE OF THE RADIO LOBE

As can be seen from Fig. 3, there is a distinct feature in the X-ray data corresponding to the Southern inner radio lobe. From its location and shape, we suggest that this could be part of a shock generated by an overpressured expanding radio lobe as seen in systems such as Cen A (Kraft et al. 2003) and NGC 3801 (Croston et al. 2007). From Fig. 3, it is clear that whilst this feature is only clearly visible around the SE edge of the radio lobe, it does outline the edge of the radio lobe clearly, and the emission is not coming from either the main galaxy or the merging galaxy to the SE. From a comparison with Cen A, where a one-sided shock is also seen, with the shock being much brighter around the S lobe than the N lobe, it seems plausible that the reason why the feature is visible here is that galaxy-galaxy interactions enhance the gas density in the region. For the following subsection, we assume, from the morphology of the feature, that it is a shock generated by the radio galaxy, and make predictions about the state of the unshocked IGM that we then test against observations.

6.1 Shock Analysis

In order to determine if the physical parameters of the galaxy and ‘shock’ are consistent with that of a region containing hot shocked gas and cooler unshocked gas, we firstly extracted a spectrum of the central 10 arcsec, containing both the galaxy and the feature in order to ensure an adequate signal-to-noise ratio to give a well-constrained fit. We then fitted this spectrum with an absorbed double APEC model in order to constrain the multiple temperatures expected in a shock model; the results of this fit are given in Table 5. We find a temperature for the hot component of the APEC model of $(1.9_{-0.3}^{+0.8})$ keV, together with the other parameters as detailed in Table 5. **Extracting a spectrum of a region containing the shock only results in a spectrum with a significantly worse signal-to-noise ratio, which, whilst still allowing a temperature to be fitted to the shock, results in a poorly constrained fit. The temperature found in this case is consistent with that found from the multi-temperature model, but very poorly constrained. Thus, we use the temperature from the multi-temperature fit in this analysis.** Further, since the galaxy temperature is consistent with the group temperature found in Section 5.2 at the $1 - \sigma$ level, we take the temperature of the group, (0.7 ± 0.1) keV to be the temperature of the unshocked gas.

Assuming that the standard Rankine-Hugoniot conditions hold, the Mach number, \mathcal{M} of the shock is given by:

$$\frac{T_2}{T_1} = \frac{[2\Gamma\mathcal{M}^2 + (1 - \Gamma)] [\Gamma - 1 + \frac{2}{\mathcal{M}^2}]}{(\Gamma + 1)^2}, \quad (1)$$

where T_2 is the temperature of the shocked gas, $1.9_{-0.3}^{+0.8}$ keV, T_1 is the downstream (unshocked) gas temperature, taken to be the group temperature, 0.7 ± 0.1 keV, and Γ is the adiabatic index, taken here to be 5/3 for a hot, non-relativistic plasma. This gives $\mathcal{M} = 2.4_{-0.5}^{+1.0}$.

We can then calculate the expected density contrast using:

$$\frac{\rho_2}{\rho_1} = \frac{\Gamma + 1}{\Gamma - 1 + \frac{2}{\mathcal{M}^2}}. \quad (2)$$

This gives an expected density contrast of $2.6_{-0.4}^{+0.6}$ between the shocked and unshocked gas. The pressure contrast is similarly given by

$$\frac{P_2}{P_1} = \frac{2\Gamma\mathcal{M}^2 + (1 - \Gamma)}{\Gamma + 1}, \quad (3)$$

and found to be 7_{-3}^{+7} .

Using the APEC normalisation N_S for the higher temperature APEC model, given in Table 5, we can calculate the density of the shocked gas component since

$$n_e = \left\{ \frac{4\pi [D_A (1 + z)]^2 N_S \times 1.18}{1 \times 10^{-14} V_S} \right\}^{\frac{1}{2}} \text{ cm}^{-3}, \quad (4)$$

where D_A is the angular size distance to the source, and V_S is the volume of the shocked gas in cm^3 . It is clear that the measured density will be strongly dependent on V_S , but the thickness of the shock cannot be determined accurately since the shock is not fully resolved in our data. Comparisons with Cen A suggest that the shock thickness should be of the order 200 pc, whilst direct measurement of the shock from the data suggests a thickness of the order of 2 kpc, although this is an upper limit, as we have not taken the *Chandra* point-spread-function (PSF) into account. We thus use these two values as limits in calculating the density of the shocked gas. We model the shock as half a hemispherical shell of inner radius corresponding to the radius of the radio lobe, measured in AIPS to be

3.4 arcsec (4.3 kpc), and outer radius as determined by the shock thickness we use. Using these densities, we can then calculate the pressure of the shocked gas using

$$P = 2.54 \times 10^{-9} n_e kT, \quad (5)$$

where n_e is the electron density of the shocked gas, kT is the temperature and P is in Pa. We show our calculated volumes, densities and pressures (n_2 and P_2 in Eqns. 2 and 3 respectively) in Table 7, together with predicted values of the corresponding unshocked quantities (n_1 and P_1).

6.2 Testing predictions from the shock analysis

If the feature seen in Fig. 3 is indeed a shock, as indicated by the significantly higher temperature of the region compared to its surroundings, then the predictions detailed in Table 7 should agree with the measured parameters of the unshocked gas. To this end, we use the density profile calculated in Section 5.1 to estimate the density of the gas that would have been swept up by the inner lobe and subsequently shocked. The gas would have been swept up from the central 3 arcsec (i.e. from within the radius of the lobe), which from Fig. 5, is in the range $0.012 - 0.15 \text{ cm}^{-3}$, consistent with our predictions in Table 7, for both values of shock thickness that we use.

Furthermore, we calculate from the radio data (see Section 3) that the minimum internal pressure of the radio lobe is $P_{min} = 6 \times 10^{-12}$ Pa, and that the central pressure of the unshocked IGM in the same region as above is in the range $0.34 - 2.0 \times 10^{-11}$ Pa. However, as the radio lobe and shock must be in pressure balance (i.e. the pressure of the radio lobe should be $2 - 12 \times 10^{-10}$ Pa), this implies that the true pressure of the radio lobe must be approximately 10-350 times greater than the minimum pressure calculated. This is consistent with what is seen in both NGC 3801 and Cen A, where the minimum pressure calculated directly from the radio lobes is far less than the shock pressure, so that the lobes must be some way from the minimum pressure condition.

Additionally, we can investigate the ways in which shock formation may be suppressed to the SW of the S radio lobe and over the whole of the N radio lobe. The lobe and the visible shock should be in pressure balance; this pressure must be constant throughout the radio lobe, and is what drives the shock. Further assuming that the N radio lobe has a similar pressure to the S radio lobe, there are then two ways in which visible shock formation can be suppressed:

(i) A shock could be formed, but could just be too faint to detect in this observation.

(ii) The external pressure and/or density could be increased to such a value that the expansion is no longer supersonic in these regions, but rather subsonic, so that no shock is formed.

In the first case if the density decreases, then so will the external pressure and in turn, the Mach number will also increase, implying a stronger shock. However, in the limit of a strong shock, the density contrast tends to 4. Using this fact, we can place limits on the density around the SW of the S lobe and the N lobe from the X-ray data.

From the data, we find that after background subtraction, there are approximately 72 counts in the shocked region. Placing similarly sized regions to the SW, NW and NE of the radio lobes, we find upper limits on the number of counts in what could be regions of shocked gas, assuming Poisson statistics, and show these limits in Table 8. Then, assuming the same conversion between counts and density in the SW, NW and NE regions as in the visibly shocked

Table 7. Estimated parameters for the shocked gas together with predicted values for the unshocked gas, assuming that standard Rankine-Hugoniot conditions apply and calculated using two different values of shock thickness (ΔR)– 0.2 kpc (by comparison with Cen A) and 2 kpc (from direct measurement).

ΔR (kpc)	V_S (cm ³)	ρ_2 (cm ⁻³)	P_2 (10 ⁻¹⁰ Pa)	Predicted ρ_1 (cm ⁻³)	Predicted P_1 (10 ⁻¹⁰ Pa)
0.2	3.6×10^{65}	0.20 ± 0.01	$9.5_{-0.8}^{+2}$	0.06–0.09	0.62–2.9
2	5.3×10^{66}	0.052 ± 0.002	$2.2_{-0.2}^{+0.5}$	0.02–0.03	0.1–0.7

region, i.e. the same temperature, we can calculate upper limits on the density as the number of counts, $N_c \propto n_e$. The calculated upper limits on shocked and unshocked density are given in Table 8. From the limits calculated, we estimate that the SE portion of the lobe could be hitting a region of the IGM which is 3-5 times denser than the surrounding medium. This increase in density could arise from interactions with the spiral galaxy to the SE, causing the shock to be visible only where it is.

Alternatively it could be the case that the external temperature or density were high enough such that the expansion no longer produced a shock. This would require the ratio between the internal and external pressures, P_{int} and P_{ext} respectively, to follow

$$\frac{P_{\text{int}}}{P_{\text{ext}}} \gtrsim \Gamma + 1, \quad (6)$$

implying that if $P_{\text{ext}} \sim 0.5P_{\text{int}}$, (i.e. if P_{ext} was increased to the range $1 - 6 \times 10^{-10}$ Pa) then a supersonic expansion would no longer occur. In this case, we would require that either the temperature would be increased (at constant density) to approximately 1.9 - 11 keV or that the density would increase (at a constant temperature of 0.7 keV) to $0.056 - 0.33 \text{ cm}^{-3}$. However, at constant temperature, this would increase the emissivity, making any emission brighter. The emissivity could be reduced if the temperature were also correspondingly reduced, but this would have the effect of making the shock stronger, and thus increasing the temperature, implying that increasing the external pressure to cause a sub-sonic expansion is probably not a viable method of suppressing shock formation in these circumstances.

It seems clear from our analysis of the unshocked gas and the regions where a shock would be expected to be seen, that the physical properties of the system are entirely consistent with the scenario presented of a young, over-pressured radio galaxy, expanding supersonically into the IGM and generating shocks in the IGM as it does so. The sidedness of the shock can be explained by variations in the IGM density, and the morphology of the elongated structure seen in the X-ray is consistent with this feature being a shock generated by the restarting radio galaxy.

7 THE RELATIONSHIP BETWEEN THE HOST GALAXY, THE RADIO PROPERTIES AND CONSEQUENCES FOR FEEDBACK

It is known that other observed young, overpressured radio sources, Cen A and NGC 3801, exhibit evidence for their host galaxies having recently undergone mergers with gas-rich galaxies (Israel 1998 and Croston et al. 2007). Furthermore, they exhibit signs of containing dusty tori (high absorbing columns are required to model the spectra accurately). This is more usually associated with powerful, high-excitation radio galaxies (generally FRIs) as described in Hardcastle et al. (2006) and Hardcastle et al. (2007), where it is argued that such sources accrete cold gas in a conventional radiatively efficient mode ('cold-mode' accretion). Recent mergers in

both Cen A and NGC 3801 could provide a reservoir of cold gas that could fuel this accretion mode.

However, whilst the host galaxy of B2 0838+32A shows signs of interactions with nearby galaxies, there is no evidence for either the host galaxy having had a recent merger, nor is there evidence for large quantities of cold gas and dust in the optical images of the host galaxy, although we do not have deep optical observations. Further, the AGN spectrum does not need a high absorbing column to accurately fit the spectrum. On the contrary, as seen in Section 5.3, the best-fitting AGN spectrum is a uniform power law with Galactic absorption, with no evidence for absorption from a dusty torus and is consistent in all ways with the class of low-excitation radio galaxies to which most FRI radio galaxies belong, and which are argued by Hardcastle et al. (2007) to be powered in a radiatively inefficient manner, termed a radiatively inefficient accretion flow, (RIAF) by direct accretion of the hot, X-ray-emitting gas. Thus, it is possible that the restarting outburst seen in B2 0838+32A is a purely heating and cooling regulated event, accreting from the hot IGM rather than from a reservoir of cold gas that has resulted from a recent merger with a gas-rich galaxy. It is probable that the previous outburst, seen at large scales, heated the gas surrounding it whilst active. This would have caused the gas around the core to expand as energy was injected into it, until such time that the gas was too tenuous to feed the AGN, effectively starving the AGN of fuel. Without excess heating from an AGN, the IGM was then able to cool radiatively until such a point that the black hole was able to accrete hot gas once more and restart the radio galaxy.

Whilst we cannot definitively rule out the presence of cold gas in the radio galaxy host, the X-ray AGN spectrum, as discussed above, rules out absorption from a dusty torus. Further deep observations in the optical and HI bands would be needed to conclusively determine that no cold gas was present, but the lack of absorption from a dusty torus is consistent with sources where it is thought that hot-mode accretion is the primary fuel of the radio source.

7.1 Feedback time-scales and dynamics of the radio sources

Using the spectral ages of the outer lobes calculated in Section 3, together with dynamical arguments, we can estimate the time-scales on which feedback processes in this system occur. From Section 3, the outer lobes are approximately $(4.6 \pm 0.2) \times 10^7$ yr old. Since this assumes the initial acceleration of a population of relativistic electrons which are then left to evolve without further re-acceleration, this time-scale can be taken to be the time when energy injection ceased, i.e. when the jets turned off, and gives a lower limit on the age of the lobes. We can then calculate an upper limit from the dynamics of the outer lobes. If we assume that they have expanded in-situ from a negligibly small radius to their current radius of approximately 65 kpc at the sound speed of the group (though it is more likely that they have expanded subsonically), then an upper limit on the age of the lobes is approximately 2×10^8 years, which obviously includes the time during which the

Table 8. Estimated upper limits on density in the regions where the shock is not detected

Region	Counts	Estimated shocked density (cm ⁻³)		Estimated unshocked density (cm ⁻³)	
		$\Delta R = 0.2$ kpc	$\Delta R = 2$ kpc	$\Delta R = 0.2$ kpc	$\Delta R = 2$ kpc
SE (visible)	72	0.20	0.052	0.06 - 0.09	0.02 - 0.03
SW	13	0.085	0.022	0.021	0.0055
NW	8	0.067	0.017	0.017	0.0043
NE	10	0.075	0.019	0.019	0.0048

jet was active and after the jet has been switched off. The large scale lobes suggest that there may be some moderate motion of the host galaxy with respect to the IGM in an east-west direction. This motion could have disrupted the jets via ram pressure as seen in narrow (and some wide) angle tailed sources. However, if the galaxy velocity is subsonic, then our energy estimates will not be significantly affected. We calculate that a galaxy velocity $v_{\text{gal}} \sim 3000$ km s⁻¹ would be required for these lobes to be a passive trail left behind by the galaxy; if this were the case, the energetics would be somewhat different, but given that this velocity is some 10 times larger than the velocity dispersion of the group calculated in Section 2, we do not regard this model as plausible.

Whilst we cannot obtain a spectral age estimate of the inner lobes, the flatter spectrum suggests that these must necessarily be younger than the outer lobes. Dynamically, we know that the lobes are expanding supersonically at $2.4_{-0.5}^{+1.0}$ times the local sound speed, which we calculate to be 330 km s⁻¹. If we further assume that the initial radius of the lobes is negligible compared to the current radius, which we take to be 4.3 kpc, then the inner lobes must be between 3.4 - 6.5 Myr old.

Furthermore, the cooling time of the gas near the centre of the group is approximately 170 Myr (assuming $kT = 0.7$ keV, the density of the gas is in the range 0.078-0.015 cm⁻³ and that energy radiates away at L_X as given in Table 4). This cooling time-scale is consistent with the available constraints on the ages of the lobe, derived above, which suggests that cooling gas could be responsible for retriggering the AGN, and that a feedback driven system, with the central AGN being responsible for heating its surroundings until it starves itself of fuel, is plausibly at work in this group.

7.2 Energetics of the inner lobes

In such a case as described above, one would expect that the power available from Bondi accretion should be able to account for the power of the inner lobes of the radio galaxy (see for instance, Hardcastle et al. 2007, who argue that hot-mode/Bondi accretion is sufficient to power all objects such as 0838+32A). Thus, by estimating the black hole mass (M_{BH}) of the host galaxy, together with suitable estimates of upper limits to the central density (n_0), an estimate can be made of the Bondi power (P_{B}) available to the radio source. We take the upper bound of the central density found in Section 5.1 as a constraint on the density of the gas available to the AGN, i.e. $n_0 = 0.1$ cm⁻³. We estimate the black hole mass using the relation between black hole mass and K-band bulge magnitude derived by Marconi & Hunt (2003)

$$\log_{10} M_{\text{BH}} = 8.21 + 1.13 \times (\log_{10} L_K - 10.9). \quad (7)$$

Obtaining an absolute K-band luminosity of $L_K = 5.1 \times 10^{11} L_{\odot}$ from the 2MASS survey, we find that $M_{\text{BH}} = 1.33 \times 10^9 M_{\odot}$. The Bondi accretion rate is given by

$$\dot{M}_{\text{B}} = \frac{\pi \rho_a G^2 M_{\text{BH}}^2}{c_s^3}, \quad (8)$$

where $c_s = \sqrt{(\Gamma kT) / (\mu m_p)}$ is the sound speed of the hot gas. We find that $\dot{M}_{\text{B}} = 0.063 M_{\odot} \text{ yr}^{-1}$, and that assuming an efficiency of 0.1, $P_{\text{B}} = 3.6 \times 10^{37}$ W. To see if hot-mode accretion could account for the power of the radio source, we can calculate the work done (W) on the IGM by the radio lobe since the internal pressure (P) of the radio lobes is known (see Table 7), and the volume (V) can be estimated from the high-resolution 4.8 GHz radio maps assuming a lobe radius of 4.3 kpc and spherical symmetry to be $9.78 \times 10^{60} \text{ m}^3$. Further assuming that the plasma is relativistic, then the work done and the energy stored in the lobes is given by:

$$W = 4PV, \quad (9)$$

from which we find that $W = (1.1 - 6.7) \times 10^{52}$ J. Furthermore, given that the Mach number of the visible shock is known, the time-scale for supersonic expansion must be in the range 3.4 - 6.5 Myr, giving a mechanical power output for the radio source of $(5.4 - 62) \times 10^{37}$ W. This is comparable with P_{B} , given the uncertainties on both the central density and M_{BH} used to calculate \dot{M}_{B} and hence P_{B} , and particularly given that our radial profile analysis could not have detected an increase in the gas density on scales smaller than a few kpc, so that the central density we estimate is really a lower limit on the density available at the Bondi radius.

7.3 Energetics of the outer lobes

In addition to calculating the work done by the inner lobes, we can also calculate the energy required to power the large outer lobes as they gently expand in order to reach pressure equilibrium. In this case, if we assume from the presence of relic jets seen at large scales, that the outer lobes were created in-situ and since the large scale jets switched off the lobes have been expanding subsonically, we can calculate the work being done on the intra-group medium (IGM) at large scales and thus compare the relative energy inputs from a radio source at different stages of evolution. From the 1.4 GHz radio maps, we calculate that the NW lobe is 100 arcsec from the centre of the group and that the S lobe is 150 arcsec from the centre, and from Fig. 5 (right), we find that the pressures at these radii are $2 - 3 \times 10^{-14}$ Pa and $1 - 2 \times 10^{-14}$ Pa respectively. We further model the lobes as ellipsoids, with the NW lobe having $a_{\text{NW}} = 80$ kpc and $b_{\text{NW}} = c_{\text{NW}} = 60$ kpc, and the S lobe having $a_{\text{S}} = 90$ kpc and $b_{\text{S}} = c_{\text{S}} = 60$ kpc. If we also assume that the lobes' initial volume is negligible compared to their current volume, the lobes are in pressure balance with the IGM and that projection does not greatly affect the lobes (projection effects would make the lobes larger but place them in a lower-pressure environment), we find that for a direct comparison with the energetics of the inner lobes using Eqn. 9, the total amount of energy supplied to the NW lobe is $8 - 12 \times 10^{51}$ J and $16 - 32 \times 10^{50}$ J to the S

lobe. It is clear that both the inner lobes, and the older outer lobes are energetically comparable, with the smaller lobes being slightly more energetic, suggesting that in both cases, the radio source is able to regulate cooling in the group atmosphere.

The total PdV work done by the outer lobes is of the order $2 - 4 \times 10^{51}$ J, and, using the limits on the age of the lobes given in Section 7.1, this implies a mean rate of energy input into the IGM of between 3×10^{35} and 3×10^{36} W. Within the uncertainties, this is very comparable to the bolometric X-ray luminosity of the group, $(3.2 \pm 0.2) \times 10^{35}$ W, which implies that the energy supplied by the outer lobes has been close to sufficient to balance radiative losses over their lifetime. However, at this phase in the source's life, any energy input from the outer lobes will be at large radii, and would not be expected to prevent the cooling of the inner parts of the hot IGM.

7.4 Implications for feedback models

As calculated and discussed in the preceding Sections, there is sufficient energy in both the small-scale and large-scale lobes to counteract the effects of radiative cooling. The shock currently being driven by the small-scale lobes will also increase the central entropy and (since the Bondi accretion rate depends on entropy, $K = T/n^{2/3}$, as $K^{-3/2}$) will slow or stop accretion on to the central black hole. However, if the lobes from the previous outburst were in fact regulating accretion, as required in feedback models, then the lobes must have grown to quite a large size before accretion stopped completely; it is not clear in this case how exactly the energy/entropy would have been provided to the accreting gas. Moreover, as discussed in Section 7.2, the current, small-scale outburst does contain enough energy to counteract cooling immediately, provided that all the energy can be injected directly where it is needed. As the outburst is still active, it is clear that there is a time delay between the injection of energy and the shutting down of accretion.

This time delay could arise either because it takes some time for the energy/entropy input from the radio source to diffuse to where it is needed, or because some time is required to drain the accretion flow even after the conditions for rapid accretion cease to be met. In general a characteristic timescale for accretion flow emptying is M/\dot{M} , where M is the mass in the accretion flow and \dot{M} is the accretion rate. For accretion from the hot phase, we can estimate that $M > \frac{4}{3}\pi R_{\text{Bondi}}^3 \rho$, and this combined with equation (8) gives a lower limit for the emptying time which is dependent only on the temperature and the central black hole mass. For a system where the temperature near the Bondi radius is 0.2 keV and the black hole has a mass of $10^9 M_{\odot}$ (see Section 7.2) we estimate that this lower limit is $\sim 2 \times 10^6$ years. While this limit is considerably less than the current source on-time, it is within an order of magnitude, and so it does not seem implausible that the timescale for the accretion flow to empty could help to account for the delay in the response of the AGN to changing external conditions. Further, any angular momentum present in the accretion flow will contribute to the mass of any gas reservoir present, increasing the reservoir emptying time above that predicted from the Bondi formula.

In addition, we have shown that the central cooling time and the time since the old source switched off are very similar; thus there is another time delay in the feedback process, involving a timescale comparable to the central cooling time. While the time delays discussed in the preceding paragraph are expected in all feedback models, the delay involving the cooling time depends on the detailed microphysics of energy/entropy transfer. However, it is

clear that the relationship between the reservoir emptying/entropy raising timescale and the cooling timescale in a given system must determine the 'on-time' and duty cycle of a particular radio source.

8 SUMMARY AND CONCLUSIONS

We have presented *Chandra* observations of the group of galaxies hosting the radio source B2 0838+32A, and having shown that the host group is a foreground group at a redshift 0.068, unassociated with the Abell cluster Abell 695, we have then investigated the interaction between the radio galaxy and its host group. Our main conclusions can be summarized as follows:

(i) From the radio morphology and spectra, we propose that radio galaxy has recently restarted, exhibiting two distinct cycles of AGN activity; an older, 'dead' source that is no longer being fueled (thought to be between 50 - 200 Myr old), and a pair of smaller, younger lobes (estimated to be between 3 - 7 Myr old).

(ii) The younger lobes are over-pressured, and expanding supersonically and driving a shock into the ISM. This shock has a Mach number of $2.4^{+1.0}_{-0.5}$, and we are able to calculate the density and pressure of the shocked gas. Further, we make predictions about the state of the unshocked gas and regions where the shock is not visible, and find that the predictions are consistent with the data.

(iii) As the radio lobe must be in pressure balance with the shock, we find that the pressure of the radio lobe is approximately 20-100 times greater than the minimum pressure calculated from radio observations alone, consistent with what is seen in Cen A and NGC 3801.

(iv) The one sided-nature of the shock, which is similar to what is seen in Cen A where the shock is much fainter around the N lobe than the S lobe, can be explained by a varying density distribution across the BGG environment, which could be caused by the interacting galaxies in this system.

(v) The older lobes have done sufficient PdV work on the IGM over their lifetime to counteract radiative cooling at large radii.

(vi) However, in contrast to Cen A and NGC 3801, it appears plausible that B2 0838+32A is not being fueled from a reservoir of cold gas arising from a merger, and neither is there any evidence for a dusty torus to fuel the accretion. Whilst further observations would be needed to definitively rule out the presence of very cold accreting gas, the absence of a dusty torus provides evidence for a radiatively inefficient warm accretion flow, establishing observationally for the first time that feedback controlled radio galaxy outbursts can give rise to entropy-changing events such as shocks in the ISM.

(vii) The energetics of the system imply that there is a time delay in stopping the accretion (and therefore turning off AGN activity) which is likely to be related either to the time taken to raise the entropy of the gas close to the black hole sufficiently to stop accretion, or to the time taken to empty the gas from the accretion flow. In addition, based on our estimates of the timescales of the multiple outbursts in the radio galaxy, we argue that the time delay for the AGN activity to restart is comparable to the cooling time of the gas at the centre of the system. We hypothesise that it is the combination of these two timescales that produces the 'on-time' and duty cycle times for a given radio source.

ACKNOWLEDGMENTS

NNJ thanks CNES (the French Space Agency) for funding. MJH thanks the Royal Society for a research fellowship. The authors would also like to thank Arif Babul for useful discussions regarding the energetics and timescales and Christian Kaiser for discussion of accretion timescales.

REFERENCES

- Abell G. O., 1958, *ApJS*, 3, 211
- Abell G. O., Corwin Jr. H. G., Olowin R. P., 1989, *ApJS*, 70, 1
- Aguerri J. A. L., Sánchez-Janssen R., Muñoz-Tuñón C., 2007, *A&A*, 471, 17
- Beers T. C., Flynn K., Gebhardt K., 1990, *AJ*, 100, 32
- Begelman M. C., 2001, in Hibbard J. E., Rupen M., van Gorkom J. H., eds, *ASP Conf. Ser. 240: Gas and Galaxy Evolution Impact of Active Galactic Nuclei on the Surrounding Medium*. pp 363–
- Birzan L., Rafferty D. A., McNamara B. R., Wise M. W., Nulsen P. E. J., 2004, *ApJ*, 607, 800
- Clarke T. E., Sarazin C. L., Blanton E. L., Neumann D. M., Kassim N. E., 2005, *ApJ*, 625, 748
- Croston J. H., Hardcastle M. J., Birkinshaw M., 2005, *MNRAS*, 357, 279
- Croston J. H., Hardcastle M. J., Birkinshaw M., Worrall D. M., Laing R. A., 2008, *ArXiv e-prints*, 802
- Croston J. H., Kraft R. P., Hardcastle M. J., 2007, *ApJ*, 660, 191
- Donato D., Sambruna R. M., Gliozzi M., 2004, *ApJ*, 617, 915
- Evans D. A., Worrall D. M., Hardcastle M. J., Kraft R. P., Birkinshaw M., 2006, *ApJ*, 642, 96
- Fabian A. C., Sanders J. S., Allen S. W., Crawford C. S., Iwasawa K., Johnstone R. M., Schmidt R. W., Taylor G. B., 2003, *MNRAS*, 344, L43
- Fabian A. C., Sanders J. S., Taylor G. B., Allen S. W., Crawford C. S., Johnstone R. M., Iwasawa K., 2006, *MNRAS*, 366, 417
- Fanti R., Gioia I., Lari C., Ulrich M. H., 1978, *A&AS*, 34, 341
- Feitsova T. S., 1981, *Soviet Astronomy*, 25, 647
- Hardcastle M. J., Evans D. A., Croston J. H., 2006, *MNRAS*, 370, 1893
- Hardcastle M. J., Evans D. A., Croston J. H., 2007, *MNRAS*, 376, 1849
- Heinz S., Brüggén M., Young A., Levesque E., 2006, *MNRAS*, 373, L65
- Israel F. P., 1998, *A&ARv*, 8, 237
- Jaffe W. J., Perola G. C., 1973, *A&A*, 26, 423
- Jetha N. N., Hardcastle M. J., Sakelliou I., 2006, *MNRAS*, 368, 609
- Jetha N. N., Ponman T. J., Hardcastle M. J., Croston J. H., 2007, *MNRAS*, 376, 193
- Kraft R. P., Vázquez S. E., Forman W. R., Jones C., Murray S. S., Hardcastle M. J., Worrall D. M., Churazov E., 2003, *ApJ*, 592, 129
- Leahy J. P., 1991, *Interpretation of large scale extragalactic jets. Beams and Jets in Astrophysics*, pp 100–
- Marconi A., Hunt L. K., 2003, *ApJL*, 589, L21
- Morganti R., Killeen N. E. B., Ekers R. D., Oosterloo T. A., 1999, *MNRAS*, 307, 750
- Noonan T. W., 1981, *ApJS*, 45, 613
- Nulsen P. E. J., McNamara B. R., Wise M. W., David L. P., 2005, *ApJ*, 628, 629
- Nusser A., Silk J., Babul A., 2006, *MNRAS*, 373, 739
- Osmond J. P. F., Ponman T. J., 2004, *MNRAS*, 350, 1511
- Owen F. N., Eilek J. A., Kassim N. E., 2000, *ApJ*, 543, 611
- Peterson J. R., Paerels F. B. S., Kaastra J. S., Arnaud M., Reiprich T. H., Fabian A. C., Mushotzky R. F., Jernigan J. G., Sakelliou I., 2001, *A&A*, 365, L104
- Popesso P., Biviano A., Böhringer H., Romaniello M., Voges W., 2005, *A&A*, 433, 431
- Reynolds C. S., Heinz S., Begelman M. C., 2002, *MNRAS*, 332, 271
- Sakelliou I., Peterson J. R., Tamura T., Paerels F. B. S., Kaastra J. S., Belsole E., Böhringer H., Branduardi-Raymont G., Ferrigno C., den Herder J. W., Kennea J., Mushotzky R. F., Vestrand W. T., Worrall D. M., 2002, *A&A*, 391, 903
- Sandage A., 1978, *AJ*, 83, 904
- Sanderson A. J. R., Ponman T. J., Finoguenov A., Lloyd-Davies E. J., Markevitch M., 2003, *MNRAS*, 340, 989
- Sarazin C. L., Rood H. J., Struble M. F., 1982, *A&A*, 108, L7
- Struble M. F., Rood H. J., 1987, *ApJS*, 63, 543
- Struble M. F., Rood H. J., 1999, *ApJS*, 125, 35
- Willis J. P., Pacaud F., Valtchanov I., Pierre M., Ponman T., Read A., Andreon S., Altieri B., Quintana H., Dos Santos S., Birkinshaw M., Bremer M., Duc P.-A., Galaz G., Gosset E., Jones L., Surdej J., 2005, *MNRAS*, 363, 675
- Wise M. W., McNamara B. R., Nulsen P. E. J., Houck J. C., David L. P., 2007, *ApJ*, 659, 1153